Rationalizing the Mechanism of Peroxyformate Decomposition: Computational Insights To Understand Solvent Influence

Diego Garay-Ruiz[a] and Carles Bo*[a, b]

Abstract: The heterolytic decomposition of *tert*-butyl peroxyformate to *tert*-butanol and carbon dioxide, catalyzed by pyridine, is a long-known example of a reaction whose kinetics are strongly affected by solvent polarity. From DFT and ab initio methods together with the SMD implicit solvation model, an extension on the formerly accepted mechanism is proposed. This novel proposal involves the formation of a carbonic acid ester intermediate and its further decomposition, through an unreported pyridine-mediated stepwise route. Computed barriers for this mechanism at DLPNO/CCSD(T)-def2-TZVP are in excellent agreement with experimental kinetic data across different solvents. Furthermore, the strong relationships between activation energies, geometric parameters in the transition state and the characteristics of the different solvents are also analyzed in depth.

Introduction

The importance of solvents in chemistry and catalysis cannot be overestimated. Apart from providing a medium to dissolve the reagents so they can come into contact, the specific features of a solvent can eventually determine many aspects about how feasible and useful the reaction is. For example, key parameters like the yield, the selectivity or the ease of purification are, in many occasions, directly controlled by the solvent of choice. Among all these possible influential factors, a recent review by Dyson and Jessop[1] focuses on the *chemical* influence of the solvents in catalysis. The preference of a catalytic system for one or other product, the overall kinetics of the reaction and the underlying reaction mechanism can be deeply altered by the solvent, thus allowing chemists to tweak the desired reactivity just by changing the reaction medium.

From the computational point of view, there has always been a deep interest on developing accurate models to mimic the effects of solvents in calculations. We can consider two main approaches for this modeling: *explicit* and *implicit* solvation models.[2,3]

In explicit models, the solvent molecules are directly considered as a part of the system, together with the solvated structures under study. This allows for a more realistic description of the system, as all the "pieces of the puzzle" are considered at once. However, it is not yet possible to model an arbitrarily large number of molecules with highly accurate methods (ab initio or DFT), as the computational cost of such calculations quickly grows with the number of atoms. Therefore, explicit solvent modeling requires either i) to limit the number of solvent molecules to consider, handling only the first solvation shells with high-cost QM methods, or ii) to resort to hybrid simulations in which most of the solvent molecules are described with a much cheaper force field (QM/MM[4,5]) or a semi-empirical QM method rather than with the more costly method used to model the reactive part of the system.

In contrast, implicit models do not consider solvent molecules, but instead try to approximate them as a continuum which surrounds the individual solutes, confined in an electrostatic cavity. This kind of approximation is much less expensive and easier to set up than explicit solvation: indeed, implicit models such as PCM,[6–8] SMD,[9] or COSMO[10] are ubiquitous in standard computational chemistry and catalysis, and thus are implemented in many electronic structure codes. Moreover, explicit approaches do also require an extensive sampling for the degrees of freedom (DOF) of the solvent, requiring statistical ensemble-based calculations and long dynamic trajectories. Implicit models overcome this issue naturally, as these DOF are averaged out for the continuum-based methods. Recently, there have been significant developments in alternative hybrid approaches for solvent modelling, such as the 3D Reference Interaction Site Model (3D-RISM).[11,12] Under this approach, solvents can be described using liquid state theories, while keeping the QM description for solutes. The molecular nature of the solvent is preserved, as in explicit models, but avoiding their sampling problems. However, it must be taken into account that neither implicit solvation nor liquid state

[a] D. Garay-Ruiz, Prof. Dr. C. Bo
Institute of Chemical Research of Catalonia (ICIQ)
Barcelona Institute of Science & Technology (BIST)
Av. Països Catalans, 16, 43007 Tarragona (Spain)
E-mail: cbo@iciq.cat

[b] Prof. Dr. C. Bo
Departament de Química Física i Inorgànica
Universitat Rovira i Virgili (URV)
C/ Marcel·lí Domingo s/n, 43007 Tarragona (Spain)

Chemistry–A European Journal

Full Paper
doi.org/10.1002/chem.202100755

Chemistry Europe
European Chemical
Societies Publishing

models will be able to handle situations in which the solvent is *directly* involved in the reaction, which can only be observed with some degree of explicit modelling. Thus, choosing one or other approach, in the end, depends strongly on the behavior of the specific system under study.

Herein, the reaction that we aim to study is the organocatalyzed *tert*-butylperoxyformate decomposition reaction proposed by R. E. Pincock in the 1960s,[13,14] also highlighted in the aforementioned review by Dyson and Jessop. This reaction (Scheme 1) shows a strong solvent dependence, working both in polar and nonpolar solvents but being much faster on the former. Experimental kinetic constant values are also available for plenty of solvents,[14] providing us a framework to compare our calculations with.

As shown in Scheme 1, pyridine assists an heterolytic decomposition of the peroxo bond leading to the formation of carbon dioxide and *tert*-butanol. Here, the organocatalyst acts as a base, capturing the proton in the *formate* group and generating a charge-separated complex involving protonated pyridine and a *tert*-butoxide anion, which would then undergo an acid-base rearrangement to form the final products.

The transition state shown in Scheme 2 shows an important degree of charge separation, as the peroxo bond is broken and the pyridine is protonated. Therefore, solvents with different polarities would have different degrees of TS stabilization, which is the alleged explanation for the important differences in reaction performance reported in the original study.[14] However, the proper characterization of transition states, which cannot be isolated experimentally, requires the aid of computational studies, which to our notice have never been applied to this system. In this report, we aim to carry out an in-depth characterization of the reaction mechanism, elucidating the corresponding structures and energies via DFT and ab initio methods, to ascertain the origin and extent of solvent effects through the SMD[9] implicit solvation model.
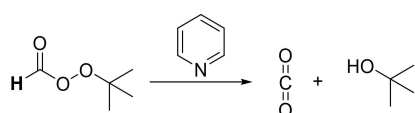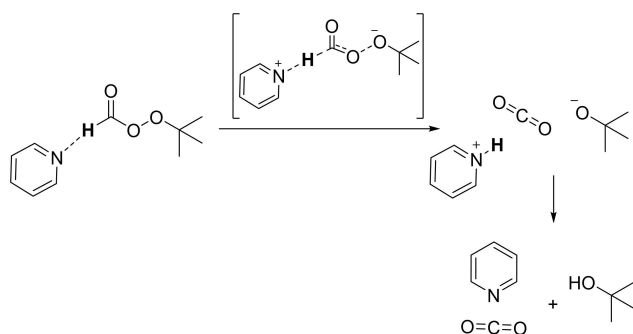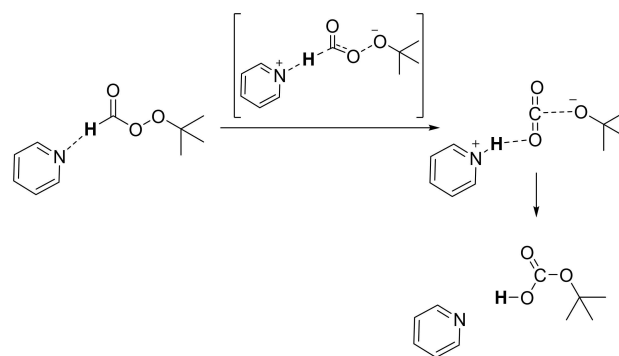
Results

A set of 29 solvents (Table 1) was selected in order to carry out the DFT characterization of the reaction. Among these, we included 15 of the solvents used in the original experimental study, excluding these for which no SMD parameters were available. As for the remaining fourteen, we included a subset of common protic solvents (water, alcohols and acids) and some additional polar solvents aiming for a better coverage of the polarity space.

A key difference with the proposed mechanism[14] appears from the very beginning of the DFT characterization: while the transition state proposed by Pincock was characterized without further problems in all tested solvents, the proposed zwitterionic product complex, involving a free *tert*-butoxide anion could not be found in most of them. This intermediate shows a very large degree of charge separation that is not expected to be accessible at all in nonpolar solvents, unable to solvate the resulting charges. In contrast, following from our calculations, we propose an alternative *carbonate* intermediate formed right from peroxo bond breaking (Scheme 3).

The formation of carbon dioxide in this proposal is merely transient: the presence of a very strong nucleophile such as

Table 1. List of solvents employed in the present study, with the corresponding dielectric constants. Different shadings are used to separate solvent groups. From the left upper corner, we have nonpolar, polar and protic solvents.

Solvent	ε	Solvent	ε
heptane	1.91	butanone	18.24
cyclohexane	2.02	acetone	20.49
CCl$_4$	2.23	*o*-nitrotoluene	25.66
p-cymene	2.23	nitrobenzene	34.80
p-xylene	2.27	acetonitrile	35.69
benzene	2.27	nitromethane	36.57
cumene	2.37	DMSO	46.83
toluene	2.37	benzyl alcohol	12.46
dibutyl ether	3.04	butan-2-ol	15.94
chloroform	4.71	ethanol	24.85
chlorobenzene	5.70	methanol	32.61
THF	7.43	formic acid	41.10
CH$_2$Cl$_2$	8.93	water	78.35
isoquinoline	11.00	formamide	108.9
pyridine	12.98		

Scheme 1. Peroxyformate decomposition.

Scheme 2. Mechanistic proposal for peroxyformate decomposition.

Scheme 3. Alternative mechanistic proposal for peroxyformate decomposition, involving carbonate formation.

Chemistry–A European Journal

Full Paper
doi.org/10.1002/chem.202100755

Chemistry Europe
European Chemical
Societies Publishing

tert-butoxide in its immediate proximity induces a CO_2 fixation process where the anion attacks the central carbon of the molecule. The resulting *hemicarbonate* anion is perfectly positioned to recapture the proton which was transferred to pyridine, forming the final *carbonate* neutral product. This whole sequence (nucleophilic attack and H-transfer) occurs in a barrierless manner just after the peroxo bond-breaking transition state, and is directly captured in the intrinsic reaction coordinate (IRC) path starting from the TS seen in Figure 1.

There is a smooth, but very pronounced decrease in energy in the negative direction of the IRC, which corresponds to the continuous process of *inversion* at the CO_2 moiety: while it does become fully linear at a given point of the curve, at the very next step it starts bonding with the alkoxydic O atom. The 'bumpy' region around IRC = −20 corresponds to the barrierless hydrogen exchange between the protonated catalyst and the anionic substrate. After this transfer, the neutral carbonic acid *tert*-butyl ester is obtained, and the deprotonated pyridine catalyst is fully regenerated.

The formation of this carbonate derivative is in context with general CO_2 fixation processes[15–20] and supposes a reasonable explanation for the occurrence of the reaction on nonpolar solvents such as heptane or benzene in which purely ionic species would be highly unstable and are not suitable reaction intermediates. As we will explain later, the carbonic ester can eventually be decomposed into the observed reaction products: *tert*-butanol and carbon dioxide.

Therefore, there is a single transition state connecting the reactants (pyridine and peroxyformate) with the proposed carbonic ester, which we have also found to be the rate-determining step of the whole process.

To analyze the energetics of the reaction, we should obtain the relative energy of that given transition state in every tested solvent. We have considered two references for that energy: i) reactants at infinite distance, computed separately, and ii)
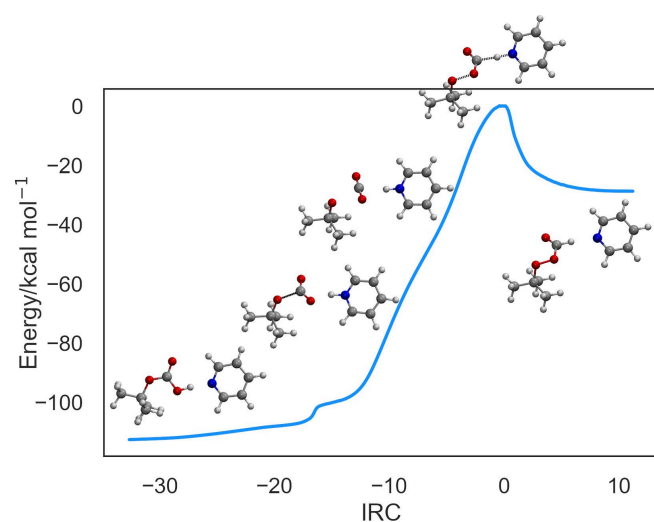
pyridine-peroxyformate reactive complex. As we will be analyzing both the *potential* and *free* activation energies, we should consider that this reactive complex is *lower* than the reactants in potential energy, but slightly *higher* in free energy.

Figure 2 highlights a very clear distinction among solvent groups as shown in the upper plot, considering reactants at infinite separation. Inspection of the individual data points in each group demonstrates that the activation energy/polarity data-driven groupings correspond perfectly with the three main solvent categories in the dataset: nonpolar (green), polar (pink) and protic (blue).

When the association complex is taken into account (lower part of Figure 2), the polar and protic groups get more mixed, due to differences in complex stabilization. Moreover, an outlier appears in the polar group (pink), corresponding to DMSO: the reactive complex in this solvent is more stabilized than in the other polar solvents, and increases the activation energy consequently.
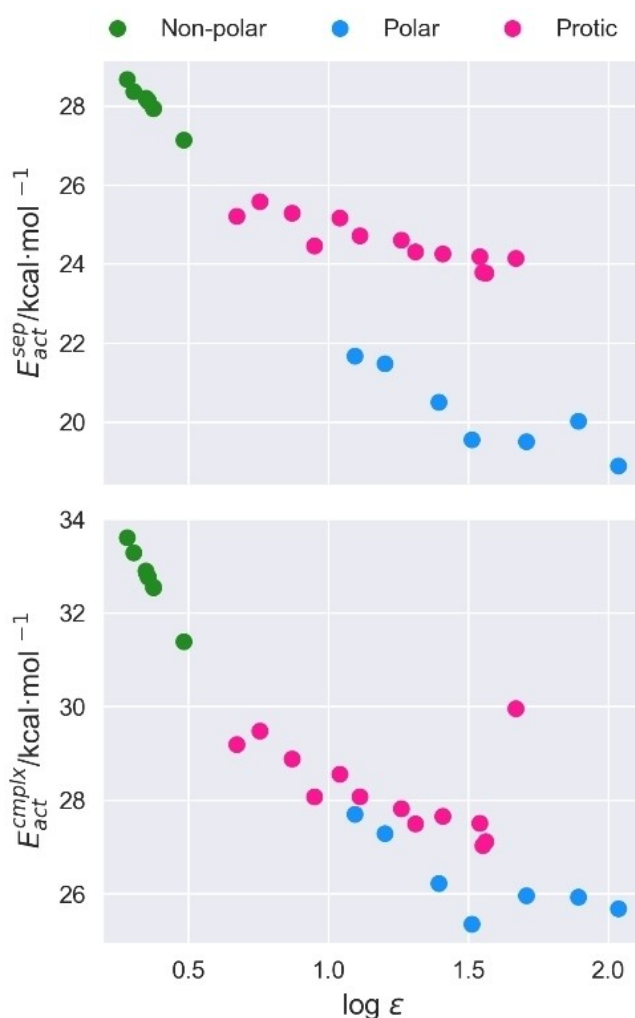

Figure 2. Potential energy barrier [kcal mol⁻¹] vs. polarity (as the logarithm of solvent's dielectric constant), considering reactants at infinite separation (above) or the association complex (below) as reference. Colors correspond to differentiated groups of solvents applying a K-Means method with three clusters on the data used for the left side of the figure.

Figure 1. IRC path for the main transition state of the reaction, with chloroform as the solvent. Potential energies [kcal·mol⁻¹] relative to the maximum (TS energy). Key 3D structures along the path are shown next to the curve.

Chemistry–A European Journal

Full Paper
doi.org/10.1002/chem.202100755

Chemistry Europe
European Chemical
Societies Publishing

Previous explanations about the changes in reaction performance across solvents[1,14] only considered the *stabilization* of the transition state, disregarding the possible differences in the stability of intermediates. To address this TS stabilization, we considered the difference between the energy of the TS in each solvent and the energy of the corresponding TS in the gas phase (no solvent).

While in terms of barriers (Figure 2) the reaction rate enhancement with increasing polarities was quite clear, the use of TS stabilization as a descriptor (Figure 3) does not work so well: above a certain polarity threshold ($\log \varepsilon > 1.2$), the transition state starts to suffer a certain degree of destabilization, which is more subtle for *polar* solvents and more pronounced for *protic* ones. Therefore, the consideration of the interplay between reactants, association complex and transition state is required to properly treat the reactivity of the system.

As experimental kinetic information is available for several of the solvents in our dataset[14], we may compare our barrier predictions with the reported rate constants. To do this, we will convert the kinetic constants to *experimental* activation free energies through the Eyring equation:

$$\Delta G^{\ddagger} = -RT\left(\log k - \log \frac{k_{B}T}{h} \right)$$

These experimental values will be compared with the free energy barriers using the *association complex* as reference, employing: i) DFT free energies, ii) DLPNO/CCSD(T) single point potential energies computed over every DFT geometry + DFT free energy correction. In this way, we get access to more accurate energies (of CCSD(T) quality) with a reasonable computational cost.

There is a very good agreement between the DLPNO/CCSD(T)-based prediction and the experimental values (Figure 4): the root mean square deviation (RMSD) between them is
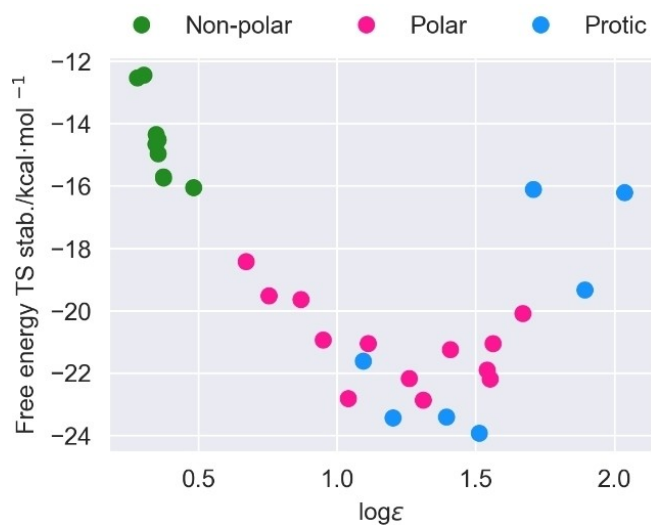

Figure 4. Comparison between experimental (*x*-axis) and computed (*y*-axis) Gibbs free activation energies [kcal·mol^{-1}] using ωB97XD (above) and DLPNO/CCSD(T) (below) values. The agreement between both energies is also depicted in a green/red color scale, with green showing a better agreement.

Figure 3. Gibbs free energy TS stabilization [kcal mol^{-1}] comparing energies optimized in solvent and in the gas phase, against the logarithm of the dielectric constant of the medium.
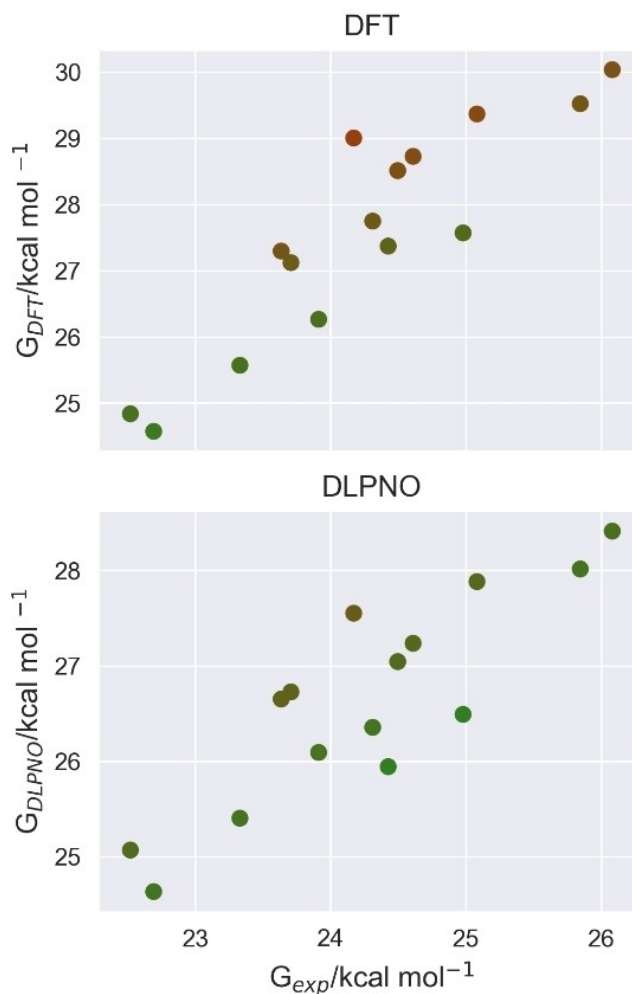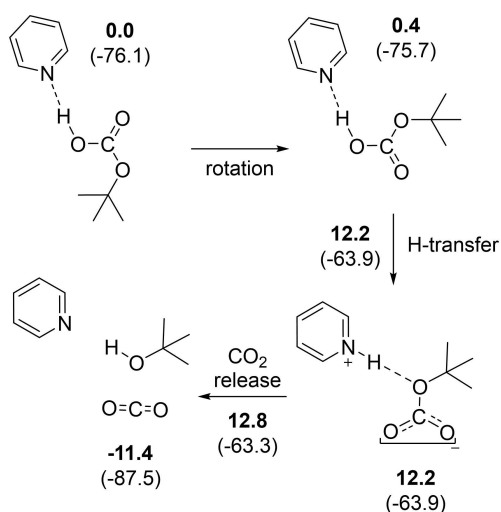
2.4 kcal mol^{-1}, with individual differences ranging between 1 and 3 kcal mol^{-1}. In contrast, the DFT-based values give a larger RMSD of 3.5 kcal mol^{-1}. We can also observe that the trend is quite linear, with a r^2 value of 0.76. The SMD solvent model, then, works quite well to model the reaction, confirming that the main contribution to the changes in reactivity comes from electrostatic effects and not from more dramatic mechanistic shifts. We should bear in mind, however, that the solvents tested in the experiments do only include *nonpolar* and *polar* solvents: we do not have any experimental information about the solvents in the *protic* group.

Regarding the decomposition of the carbonic acid ester into the observed reaction products (carbon dioxide and *tert*-butanol), a direct transformation with unassisted proton migration to the —O—tBu group is not accessible: the corresponding TS is 37.4 kcal mol^{-1} above the carbonic ester in chloroform.

Chemistry–A European Journal

Full Paper
doi.org/10.1002/chem.202100755

**Chemistry
Europe**
European Chemical
Societies Publishing

This is in agreement with general trends for the reactivity of carbonic acid derivatives, which do not generally decompose through this kind of four-membered ring TS. Nonetheless, pyridine can indeed catalyze the reaction, opening a low-energy route (Scheme 4).

The strong interactions between the acid group and the basic pyridine moiety keep both units close, and allow the acid hydrogen atom to be passed back and forth between N and O. Indeed, the H-transfer transition state and the ion pair intermediate are almost *isoenergetic* in terms of Gibbs free energy at this level of calculation (both at 12.2 kcal mol^{-1}).

Potential energies, in contrast, effectively confirm this transition state to be slightly above the corresponding intermediate (10.6 vs. 10.4 kcal mol^{-1}). Through a small repositioning of the pyridinic group, it becomes possible to transfer the proton to the *tert*-butyl-bearing oxygen and trigger the release of carbon dioxide, with a completely accessible barrier (12.8 kcal mol^{-1}). Moreover, the small separation between the charged units (high degree of ion pairing) explains how the decomposition occurs without issues even in nonpolar solvents. Indeed, the pyridine-catalyzed channel is much lower in energy than the analogous pathways assisted by *tert*-butanol (product autocatalysis, requiring 20.2 kcal mol^{-1}) or water (19.2 kcal mol^{-1}; Figure S4). To our notice, this kind of pyridine-mediated decomposition of a carbonic acid derivative has not been reported before. Generally, these processes are usually considered to be catalyzed by amphoteric structures capable of simultaneous proton donation and proton capture, such as water, acids, alcohols or ammonia.[21–24] In contrast, we propose a *stepwise* mechanism in which the acid is deprotonated first, leading to an intermediate ion pair. This ion pair readily undergoes decomposition, recovering the base and forming the corresponding alcohol. Compared with the *tert*-butoxide/pyridine zwitterion proposed in the original mechanism, the hemicarbonate is much less strongly nucleophilic. Then, the

comparable basicities of pyridine and hemicarbonate allow them to somehow "share" the proton, accounting for the subtle motion and interplay observed in our calculations.

As a final observation about the mechanism, an addition reaction to pyridine can be proposed instead of the former decomposition (Scheme 5). This process involves the loss of aromaticity in the pyridine ring, obtaining a secondary amine, and supposes the deactivation of the organocatalyst.

Depending on the solvent, the barrier for this addition process, computed from the carbonic acid ester, lies between 25 and 35 kcal mol^{-1}, while the product is, by all means, much less stable than the main reaction products CO_2 and *t*BuOH. Consequently, the extent of this organocatalyst-deactivating reaction is expected to be minimal: pyridine remains in the medium and allows the reaction to proceed as observed.

Figure 5 shows all free energy profiles, including our 29 different solvents, as a final summary of the energetic analysis.

Apart from clarifying the relative magnitudes of the barriers, we can also observe how energy differences due to solvent polarities are clearly larger in the charge-separated TS than in the reactant complex or in the carbonate ester intermediate.

Scheme 5. Alternative carbonate transformation route.

Scheme 4. Pyridine-catalyzed decomposition of the carbonic acid ester. Gibbs free energies [kcal mol^{-1}] referenced to the initial carbonate (above and bold) or to the separated reactants (below). Calculations were performed with chloroform as the implicit solvent.
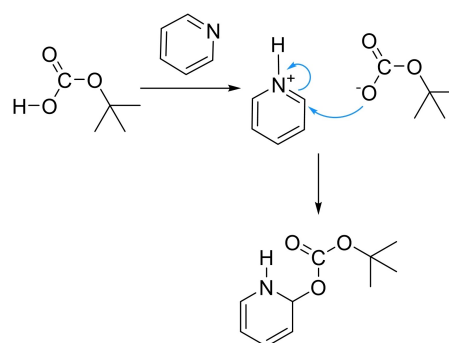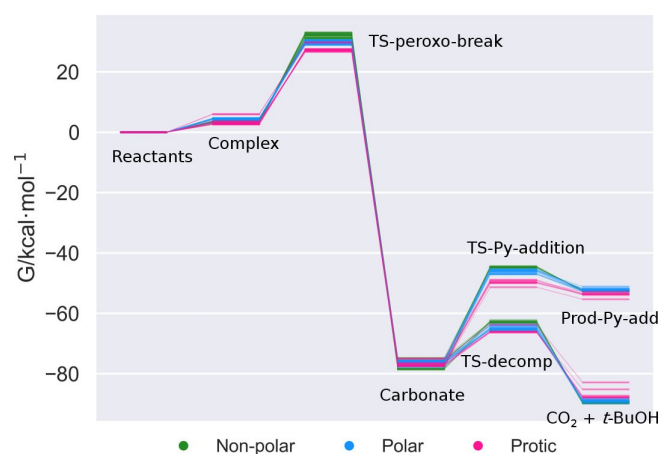

Figure 5. Gibbs free energy profiles for all solvents [kcal mol^{-1}]. Colors refer to solvent groups: green: nonpolar, pink: polar, blue: protic. The usual decomposition pathway is compared with the nucleophilic attack on pyridine shown in Scheme 5.
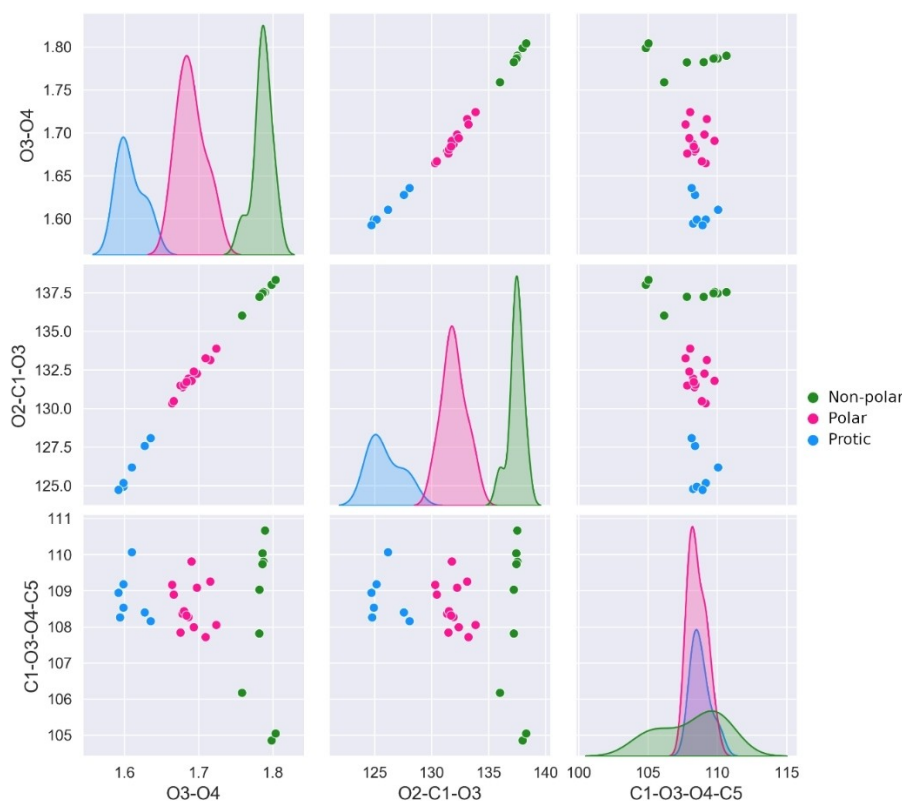
Chemistry–A European Journal

Full Paper
doi.org/10.1002/chem.202100755

Chemistry Europe
European Chemical
Societies Publishing

Figure 6. Correlation and density plots for key geometric parameters in the transition state. Starting from the top: peroxo bond length, carbonate OCO angle and COOC dihedral angle for rotation around peroxo group.

This is in line with the initial hypothesis of TS stabilization being the key factor in the solvent dependency: however, the contribution of the more subtle changes in the other involved species cannot be disregarded by any means.

In all cases, as expected, decomposition of the carbonate into the experimental products (carbon dioxide and *tert*-butanol) is thermodynamically favorable, although it can be also seen that for protic solvents (in blue) this difference becomes less pronounced.

Also, while the proposed catalyst deactivation (Scheme 5) is clearly disfavored for all solvents, important kinetic differences are shown, with barriers being much lower again in *protic* solvents.
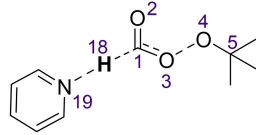
Another aspect which seems worth analyzing is the extent of geometric differences among the transition states optimized with different solvents, determining whether the observed energy differences are merely a question of solvation energy or if there is some kind of fundamental change in TS structure depending on solvent polarity. To do this, we selected a set of relevant bond lengths, angles and dihedral angles that are affected by the reaction (Table 2) and considered *correlation plots* among them to highlight possible geometric trends (Figure 6).

Figure 6 shows major differences across the previously identified solvent groups. In nonpolar solvents (green), we have that the peroxo bond is more broken and the OCO angle is closer to linearity, that is, closer to CO_2 release. In polar (pink) and especially protic (blue) solvents, in contrast, both the OCO angle and the peroxo bond remain very close to their values in the initial reactant complex. There does not seem to be rotation around the peroxo bond: all three groups are centered around the same value (109°), although the nonpolar group is slightly more spread out.

The other tested parameters show pretty much the same behavior and have been omitted for brevity: see Figure S1 for more details.

We did also consider the direct comparison of the key O–O bond length at the transition state with the *polarity* of the solvent (Figure 7). Once again, we observe an excellent separation across the nonpolar, polar and protic groups, almost

Table 2. Geometric parameters selected for analysis. The involved atoms are tagged in the 2D visualization of the transition state.

Distances	Angles	Dihedral angles
N(19)–H(18)	O(2)–C(1)–O(3)	C(1)–O(3)–O(4)–CtBu(5)
H(18)–C(1)	H(18)–C (1)–O(2)	
C(1)–O(3)	N(19)–H(18)–O(2)	
O(3)–O(4)		

Chemistry–A European Journal

Full Paper
doi.org/10.1002/chem.202100755

Chemistry Europe
European Chemical
Societies Publishing

Figure 7. Peroxo bond length [Å] vs. the logarithm of the dielectric constant of the solvent.

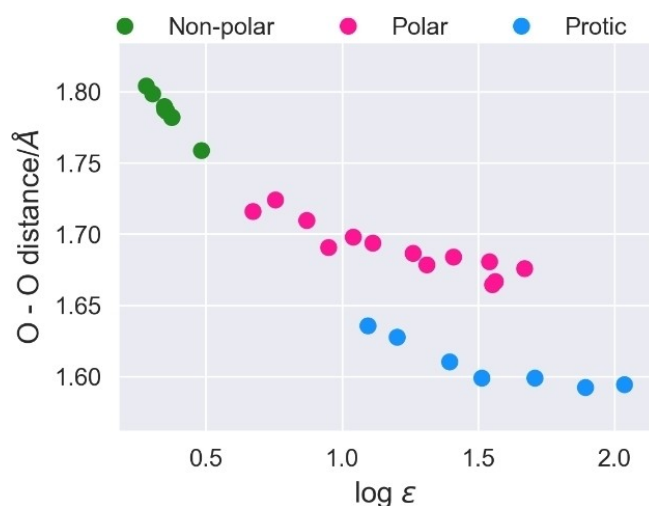**Figure 8.** Computed dipole moments for the peroxo bond-breaking transition state [Debye] vs. the logarithm of the dielectric constant of the solvent.

perfectly mimicking the shape of the initial activation energy plot (Figure 2). In fact, the direct correlation between the two variables is very close to a straight line ($r^2 = 0.97$; Figure S3). From there, we have that the peroxo bond length shows as the main factor controlling the activation energy: barriers are smaller when the O—O bond is shorter and therefore closer to the reactants, as in *protic* solvents. *Nonpolar* media have a more broken peroxide, losing stability and consequently increasing the activation energy. Analogous plots can be obtained from other geometric parameters such as the OCO bond angle (Figure S2), which is modified alongside the O—O bond.

To explain why lower-polarity solvents favor seemingly *later* transition states where the peroxo bond is longer, we should consider the module of the dipole moment of the corresponding structure, and how it correlates with solvent polarity (Figure 8).

As expected, the dipole moment is *smaller* in nonpolar solvents, while in polar solvents the computed value increases smoothly with the logarithm of the dielectric constant. The protic solvents clearly depart from the rest, with much larger dipole moments that grow very quickly with $\log\varepsilon$. Just as we observed the similarity between activation energy and O—O bond length (Figures 2 and 7), we have another strong relationship between the dipole moment and the H—C bond length: Figures 8 and 9.

The large similarity between both plots shows that, just like O—O bond length controlled the activation energy, C—H bond length controls the overall dipole moment (quasi-linear correlation, with $r^2 = 0.97$; Figure S3). Longer C—H bonds imply a larger degree of proton transfer from the formate group to the pyridine, and thus a larger degree of charge separation on the system. Therefore, protic solvents, more capable of stabilizing separated charges, allow the transition state to have larger dipole moments. The C—H bond then becomes remarkably longer than in nonpolar solvents, where the degree of proton transfer at the TS is much smaller.
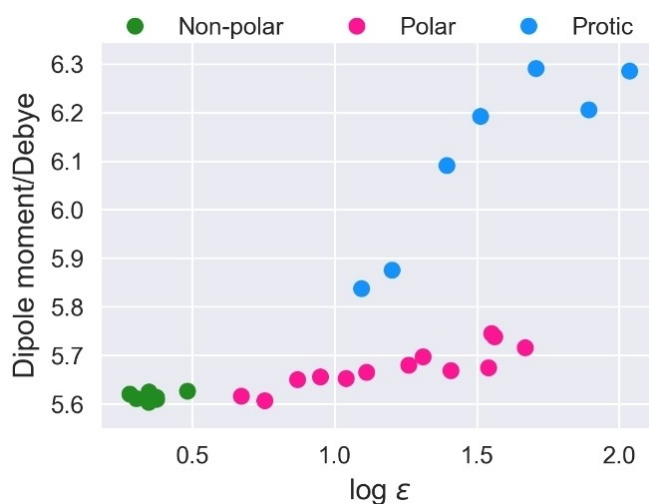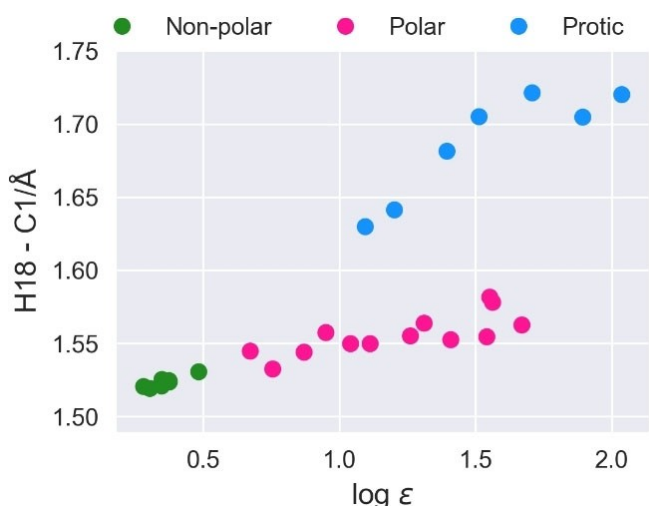

Figure 9. Hydrogen-carbon bond length [Å] vs. the logarithm of the dielectric constant of the solvent.

All in all, we see that the solvent-based differences eventually depend on the balance between the key O—O and H—C bond lengths that are altered as the reaction goes on: we cannot talk about earlier or later transition states, as the way in which the reaction occurs differs between solvents. For *protic* media, the process starts by breaking the *formate* group and transferring the hydrogen atom, while the peroxo bond in the TS remains almost intact. *Nonpolar* solvents, instead, cannot afford such a large degree of charge separation, and keep the H—C bond length and the dipole moment lower: the reaction starts then by breaking the *peroxide* group, which eventually increases the activation energy. Finally, the solvents in the *polar* group show a more *synchronous* mechanism in which both bonds are affected at once. Therefore, it shows that is the fine-tuning of the geometry of the rate-determining transition state

Chemistry–A European Journal

Full Paper
doi.org/10.1002/chem.202100755

**Chemistry
Europe**
European Chemical
Societies Publishing

which explains the fine-tuning of reaction performance across different solvents observed in the experiments.

Conclusions

Building on the initial mechanistic proposal by Pincock, we have been able to reveal several new aspects about peroxyformate decomposition through computational characterization of the free energy landscape. Moreover, we propose an analysis of solvation effects founded on the basis of geometry and energy changes in key intermediates and transition states along many different solvents.

First of all, we propose the formation of a carbonic acid *tert*-butyl ester intermediate; this was not present in the original mechanism. The formation of this neutral intermediate is more in line with the feasibility of the reaction in nonpolar solvents like heptane or benzene, where a free *tert*-butoxide anion will be far too unstable. Moreover, it allows this decomposition process to be fitted in the context of CO_2 fixation chemistry, where it is known that strong nucleophiles such as alkoxides are effective for the activation of the usually inert carbon dioxide molecule.

For the transformation of the intermediate ester into the experimentally observed products, we are also proposing a previously unreported route for the decomposition of carbonic acid derivatives. Instead of a concerted step mediated by a bifunctional structure, we have explored a low-energy stepwise pathway mediated by pyridine, the same organocatalyst prompting the peroxo bond-breaking. This stepwise pathway has been shown to be more accessible than the equivalent concerted channels mediated by water or *tert*-butanol.

A possible pathway for organocatalyst deactivation, via addition on the pyridine ring, has also been computed. While this side reaction is not competitive with the main decomposition process, it still remains relevant as a previously unexplored reaction channel in a scarcely studied system.

Regarding the extent of solvent effects, our current calculations are in very good agreement with the experimental data reported in Pincock's original study. The computed barriers are very close to the experimental values, with a RMSD value of 2.4 kcal mol^{-1} for the DLPNO/CCSD(T) energies with implicit solvent. Through a detailed analysis of both energetic and geometric parameters on the peroxo bond-breaking transition state, we have revealed strong relationships that go beyond a simple dependency on polarity, by showing how both activation energy and O–O bond length allow the main groups of solvents in the set to be "rediscovered", discriminating between nonpolar, polar and protic solvents. These differences have been rationalized through the module of the dipole moment, showing how, as expected, less-polar solvents favor transition-state structures with smaller dipole moments. Moreover, we have also shown the strong correlation between this dipole moment and the C–H bond length, completing the description of the microscopic origin of the changes in reaction performance: peroxyformate decomposition can start either with peroxide decomposition or with formate decomposition, depending on the nature and polarity of the solvent.

Computational Details

Geometry optimizations, frequency calculations and IRC analyses were carried out with the ωB97XD[25] functional and the 6-311G-(d,p) basis set,[26,27] employing Gaussian09,[28] using the built-in SMD parameters for a total of 29 solvents. Furthermore, DLPNO/CCSD(T)/def2-TZVP[29,30] single-point calculations were performed with ORCA 4.0[31,32] over selected DFT-optimized geometries for each solvent, to assess the accuracy of the DFT calculations against a higher-quality ab-initio method. Reported Gibbs free energies include standard-state corrections (assuming 1.0 M concentration) and a temperature of 90 °C, for comparison with the kinetic results from R.E. Pincock.

The nature of all minima and saddle points in the potential energy surface was confirmed through harmonic vibrational frequency analysis.

Correlation plots (Figures 6 and S1) were generated with the pairplot function in the seaborn Python library.[33]

A data set collection of computational results is available in the ioChem-BD[34] repository and can be accessed at https://doi.org/10.19061/iochem-bd-1-198.

Conflict of Interest

The authors declare no conflict of interest.

[1] P. J. Dyson, P. G. Jessop, *Catal. Sci. Technol.* **2016**, *6*, 3302–3316.
[2] J. Zhang, H. Zhang, T. Wu, Q. Wang, D. van der Spoel, *J. Chem. Theory Comput.* **2017**, *13*, 1034–1043.
[3] B. Mennucci, S. Canuto, *Challenges and Advances in Computational Chemistry and Physics*, Springer, Dordrecht, **2008**, pp. 1–21.
[4] R. E. Bulo, B. Ensing, J. Sikkema, L. Visscher, *J. Chem. Theory Comput.* **2009**, *5*, 2212–2221.
[5] T. Jiang, S. Simko, R. E. Bulo, *J. Chem. Theory Comput.* **2018**, *14*, 3943–3954.
[6] S. Miertuš, E. Scrocco, J. Tomasi, *Chem. Phys.* **1981**, *55*, 117–129.
[7] S. Miertus̃, J. Tomasi, *Chem. Phys.* **1982**, *65*, 239–245.
[8] J. L. Pascual-Ahuir, E. Silla, I. Tuñon, *J. Comput. Chem.* **1994**, *15*, 1127–1138.
[9] A. V. Marenich, C. J. Cramer, D. G. Truhlar, *J. Phys. Chem. B* **2009**, *113*, 6378–6396.
[10] A. Klamt, *J. Phys. Chem.* **1995**, *99*, 2224–2235.

[11] S. Gusarov, T. Ziegler, A. Kovalenko, *J. Phys. Chem. A* **2006**, *110*, 6083–6090.

[12] G. Jeanmairet, M. Levesque, D. Borgis, *J. Chem. Theory Comput.* **2020**, *16*, 7123–7134.

[13] R. E. Pincock, *J. Am. Chem. Soc.* **1962**, *84*, 312–313.

[14] R. E. Pincock, *J. Am. Chem. Soc.* **1964**, *86*, 1820–1826.

[15] M. North, R. Pasquale, *Angew. Chem. Int. Ed.* **2009**, *48*, 2946–2948, *Angew. Chem.* **2009**, 121, 2990–2992; *Angew. Chem. Int. Ed.* **2009**, *48*, 2946–2948

[16] M. North, R. Pasquale, C. Young, *Green Chem.* **2010**, *12*, 1514–1539.

[17] A. Decortes, A. M. Castilla, A. W. Kleij, *Angew. Chem. Int. Ed.* **2010**, *49*, 9822–9837, *Angew. Chem.* **2010**, 122, 10016–10032; *Angew. Chem. Int. Ed.* **2010**, *49*, 9822–9837

[18] C. J. Whiteoak, N. Kielland, V. Laserna, F. Castro-Gomez, E. Martin, E. C. Escudero-Adán, C. Bo, A. W. Kleij, *Chem. Eur. J.* **2014**, *20*, 2264–2275.

[19] J. González-Fabra, F. Castro-Gómez, W. M. C. Sameera, G. Nyman, A. W. Kleij, C. Bo, *Catal. Sci. Technol.* **2019**, *9*, 5433–5440.

[20] C. Maquilón, B. Limburg, V. Laserna, D. Garay-Ruiz, J. González-Fabra, C. Bo, M. Martínez Belmonte, E. C. Escudero-Adán, A. W. Kleij, *Organometallics* **2020**, *39*, 1642–1651.

[21] C. S. Tautermann, A. F. Voegele, T. Loerting, I. Kohl, A. Hallbrucker, E. Mayer, K. R. Liedl, *Chem. Eur. J.* **2002**, *8*, 66–73.

[22] M. Kumar, D. H. Busch, B. Subramaniam, W. H. Thompson, *J. Phys. Chem. A* **2014**, *118*, 5020–5028.

[23] B. Bandyopadhyay, P. Biswas, P. Kumar, *Phys. Chem. Chem. Phys.* **2016**, *18*, 15995–16004.

[24] S. Mallick, S. Sarkar, B. Bandyopadhyay, P. Kumar, *Comput. Theor. Chem.* **2018**, *1132*, 50–58.

[25] J. da Chai, M. Head-Gordon, *Phys. Chem. Chem. Phys.* **2008**, *10*, 6615–6620.

[26] R. Krishnan, J. S. Binkley, R. Seeger, J. A. Pople, *J. Chem. Phys.* **1980**, *72*, 650–654.

[27] A. D. McLean, G. S. Chandler, *J. Chem. Phys.* **1980**, *72*, 5639–5648.

[28] M. J. Frisch, G. W. Trucks, H. B. Schlegel, G. E. Scuseria, M. A. Robb, J. R. Cheeseman, G. Scalmani, V. Barone, B. Mennucci, G. A. Petersson, H. Nakatsuji, M. Caricato, X. Li, H. P. Hratchian, A. F. Izmaylov, J. Bloino, G. Zheng, J. L. Sonnenberg, M. Hada, M. Ehara, K. Toyota, R. Fukuda, J. Hasegawa, M. Ishida, T. Nakajima, Y. Honda, O. Kitao, H. Nakai, T. Vreven, J. A. Montgomery Jr., J. E. Peralta, F. Ogliaro, M. Bearpark, J. J. Heyd, E. Brothers, K. N. Kudin, V. N. Staroverov, R. Kobayashi, J. Normand, K. Raghavachari, A. Rendell, J. C. Burant, S. S. Iyengar, J. Tomasi, M. Cossi, N. Rega, J. M. Millam, M. Klene, J. E. Knox, J. B. Cross, V. Bakken, C. Adamo, J. Jaramillo, R. Gomperts, R. E. Stratmann, O. Yazyev, A. J. Austin, R. Cammi, C. Pomelli, J. W. Ochterski, R. L. Martin, K. Morokuma, V. G. Zakrzewski, G. A. Voth, P. Salvador, J. J. Dannenberg, S. Dapprich, A. D. Daniels, O. Farkas, J. B. Foresman, J. V. Ortiz, J. Cioslowski, D. J. Fox, *Gaussian 09 Revision C.01* **2010**, Gaussian Inc., Wallingford CT.

[29] D. G. Liakos, M. Sparta, M. K. Kesharwani, J. M. L. Martin, F. Neese, *J. Chem. Theory Comput.* **2015**, *11*, 1525–1539.

[30] D. G. Liakos, F. Neese, *J. Chem. Theory Comput.* **2015**, *11*, 4054–4063.

[31] F. Neese, *Wiley Interdiscip. Rev.: Comput. Mol. Sci.* **2012**, *2*, 73–78.

[32] F. Neese, *Wiley Interdiscip. Rev.: Comput. Mol. Sci.* **2018**, *8*, e1327.

[33] M. Waskom, The Seaborn Development Team, **2020**, https://doi.org/10.5281/zenodo.592845.

[34] M. Álvarez-Moreno, C. de Graaf, N. López, F. Maseras, J. M. Poblet, C. Bo, *J. Chem. Inf. Model.* **2015**, *55*, 95–103.